Fabricating three dimensional nanostructures using two photon lithography in a single exposure step

Seokwoo Jeon, Viktor Malyarchuk, and John A. Rogers*

Department of Materials Science and Engineering, Electrical and Computer Engineering, and Chemistry, Beckman Institute and Seitz Materials Research Laboratory, University of Illinois, Urbana, IL 61801
jrogers@uiuc.edu

Gary P. Wiederrecht

Chemistry Division and Center for Nanoscale Materials, Argonne National Laboratory, Argonne, IL 60439
wiederrecht@anl.gov

Abstract: Conformable phase masks, transparent photopolymers and two photon effects provide the basis for a simple, parallel lithographic technique that can form complex, but well defined three dimensional (3D) nanostructures in a single exposure step. This paper describes the method, presents examples of its ability to form 3D nanostructures (including free standing particles with controlled shapes) and comprehensive modeling of the associated optics. Single step, large area 3D pattern definition, sub-wavelength resolution and experimental simplicity represent features that make this method potentially useful for applications in photonics, biotechnology and other areas.

References

1. S. Y. Lin, J. G. Fleming, and E. Chow, "Two- and three-dimensional photonic crystals built with VLSI tools," Mrs Bulletin **26**, 627-631 (2001).
2. J. Zaumseil, M. A. Meitl, J. W. P. Hsu, B. R. Acharya, K. W. Baldwin, Y. L. Loo, and J. A. Rogers, "Three-dimensional and multilayer nanostructures formed by nanotransfer printing," Nano. Lett. **3**, 1223-1227 (2003).
3. M. Campbell, D. N. Sharp, M. T. Harrison, R. G. Denning, and A. J. Turberfield, "Fabrication of photonic crystals for the visible spectrum by holographic lithography," Nature **404**, 53-56 (2000).
4. B. T. Holland, C. Blanford, and A. Stein, "Synthesis of macroporous minerals with highly ordered three-dimensional arrays of spheroidal voids," Science **281**, 538-540 (1998).
5. S. H. Park and Y. Xia, "Fabrication of Three-Dimensional Macroporous Membranes with Assemblies of Microspheres as Templates," Chem. Mater. **10**, 1745-1747 (1998).
6. O. D. Velev, T. A. Jede, R. F. Lobo, and A. M. Lenhoff, "Porous silica via colloidal crystallization," Nature **389**, 447-448 (1997).
7. F. S. Bates, "Polymer-polymer phase behavior," Science **251**, 898-905 (1991).
8. Y. Fink, A. M. Urbas, M. G. Bawendi, J. D. Joannopoulos, and E. L. Thomas, "Block copolymers as photonic bandgap materials," J. Lightwave Technol. **17**, 1963-1969 (1999).
9. B. Michel, A. Bernard, A. Bietsch, E. Delamarche, M. Geissler, D. Juncker, H. Kind, J. P. Renault, H. Rothuizen, H. Schmid, P. Schmidt-Winkel, R. Stutz, and H. Wolf, "Printing meets lithography: Soft approaches to high-resolution printing," IBM J. Res. Dev. **45**, 697-719 (2001).
10. D. G. Grier, "A revolution in optical manipulation," Nature **424**, 810-816 (2003).
11. H.-B. Sun and S. Kawata, "Two-photon photopolymerization and 3D lithographic microfabrication," Adv. Polym. Sci. **170**, 169-273 (2004).
12. T. Kondo, S. Matsuo, S. Juodkazis, and H. Misawa, "Femtosecond laser interference technique with diffractive beam splitter for fabrication of three-dimensional photonic crystals," Appl. Phys. Lett. **79**, 725-727 (2001).
13. S. Jeon, E. Menard, J.-U. Park, J. Maria, M. Meitl, J. Zaumseil, and J. A. Rogers, "Three-dimensional nanofabrication with rubber stamps and conformable photomasks," Adv. Mater. **16**, 1369-1373 (2004).

14. S. Jeon, J.-U. Park, R. Cirelli, S. Yang, C. E. Heitzman, P. V. Braun, P. J. A. Kenis, and J. A. Rogers, "Fabricating complex three-dimensional nanostructures with high-resolution conformable phase masks," Proc. Natl. Acad. Sci. U. S. A. **101**, 12428-12433 (2004).
15. H. Schmid and B. Michel, "Siloxane Polymers for High-Resolution, High-Accuracy Soft Lithgraphy," Macromolecules **33**, 3042-3049 (2000).
16. Y. N. Xia and G. M. Whitesides, "Soft lithography," Annu. Rev. Mater. Sci. **28**, 153-184 (1998).
17. Y. G. Y. Huang, W. X. Zhou, K. J. Hsia, E. Menard, J. U. Park, J. A. Rogers, and A. G. Alleyne, "Stamp collapse in soft lithography," Langmuir **21**, 8058-8068 (2005).
18. K. J. Hsia, Y. Huang, E. Menard, J. U. Park, W. Zhou, J. Rogers, and J. M. Fulton, "Collapse of stamps for soft lithography due to interfacial adhesion," Appl. Phys. Lett. **86**, 154106 (2005).
19. S. Denizligil, R. Resul, Y. Yagci, C. McArdle, and J. P. Fouassier, "Photosensitized cationic polymerization using allyl sulfonium salt," Macromol. Chem. Phys. **197**, 1233-1240 (1996).
20. G. Witzgall, R. Vrijen, E. Yablonovitch, V. Doan, and B. J. Schwartz, "Single-shot two-photon exposure of commercial photoresist for the production of three-dimensional structures," Opt. Lett. **23**, 1745-1747 (1998).
21. "The GSOLVER ver. 4.20 developed by Grating Solver Development Company (P.O. Box 353, Allen, TX 75013)."
22. M. V. Klein, *Optics* (John Wiley & Sons, INC., New York, 1970), pp. 415-481.
23. S. Y. Chou and W. Y. Deng, "Subwavelength Amorphous-Silicon Transmission Gratings And Applications In Polarizers And Waveplates," Appl. Phys. Lett. **67**, 742-744 (1995).

1. Introduction

Many forms of nanotechnology in photonics, biotechnology, information storage and other areas require three dimensional (3D) structures with feature sizes in the deep sub-micron or nanometer range. Sequential application of conventional[1] or printing[2] based lithographic steps can build, in layer by layer strategies, certain architectures with some 3D features. Alternative methods based on interference lithography,[3] colloidal sedimentation,[4-6] polymer phase separation[7, 8] and transfer printing[2, 9] provide direct routes to certain classes of structures with true 3D character. Two or multiphoton effects can also generate such structures, but with nearly arbitrary geometries and with feature sizes as small as 100-200 nm. Patterning typically proceeds by scanning a tightly focused laser beam in, for example, a photopolymer that is crosslinked with a photocatalyst that is activated through a multiphoton process. The serial nature of this method, however, leads to relatively slow patterning speeds. Current research seeks to establish new approaches, such as those that use parallel scanning of a large number of beams generated using diffractive optics, that avoid this problem.[10] The use of two photon process in interference lithography has been proposed, but the need for ultrashort pulses and their associated broad bandwidth makes this type of patterning almost impossible;[11] only two dimensional or very limited 3D structures[12] are reported.

This paper presents a form of 3D two photon lithography that can generate certain important classes of nanostructures in a single exposure step. In this method, passage of unfocused laser pulses through transparent phase masks with subwavelength structures of relief on their surfaces generates complex, but well defined 3D distributions of intensity near the surfaces of the masks. These intensity distributions expose thick layers of transparent photopolymers that have some two photon sensitivity. The phase masks are key elements of this approach; because they are conformable, they can achieve reproducible, intimate contacts with flat solid surfaces in reversible manner, without the application of pressure. The near and 'proximity' field exposure geometries enabled by this type of physical contact and the range of relief structures that are possible on these conformable masks enable significant control over the patterning process when one photon effects are exploited for the patterning.[13, 14] This paper demonstrates that this exposure geometry enables two photon effects to be exploited in a way that retains the attractive features of the one photon process but provides a substantially increased range of 3D structure geometries that can be achieved. In the following, we show some of the features of the method by presenting structures formed by one and two photon effects using a single phase mask. Results from a variety of other masks illustrate some of the classes of 3D structures that are possible with the two photon approach. Calculations that use rigorous coupled wave analysis quantitatively capture the

essential optical effects and provide accurate predictions of the geometries of the fabricated structures, including subtle aspects such as polarization dependent behaviors.

2. Numerical calculations and measurements
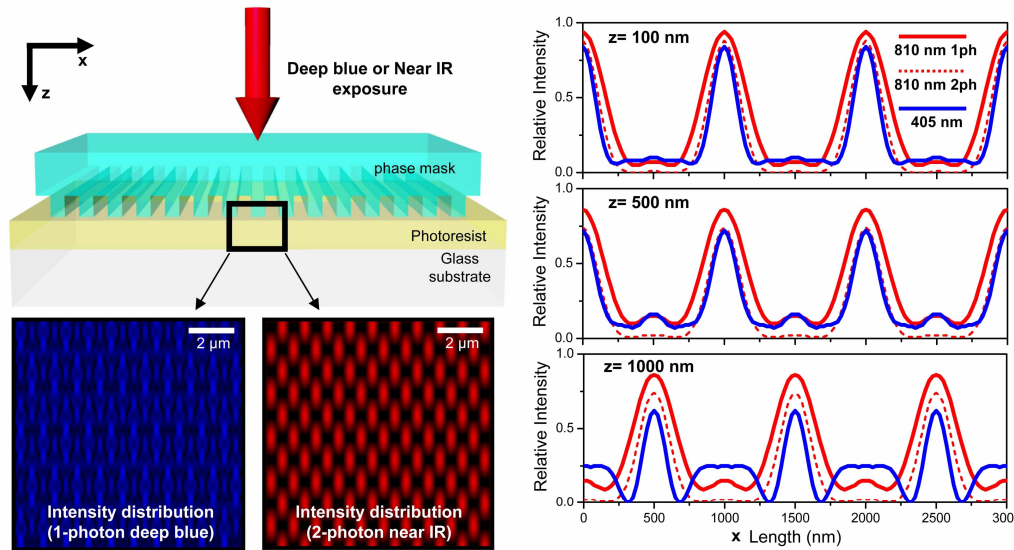
Fig. 1. Schematic illustration of the experimental setup (top frame) with a grating mask (500 nm line and space with relief depths of 510 nm and an index of refraction of 1.4). The middle frames show calculated intensity distributions in air, for two different wavelengths (blue: 405 nm exposure, red: 810 nm exposure). The bottom frames compare intensities (1 ph) and the square of the intensity (2 ph) at specific depths, z, from grating; 100, 500, and 1000 nm.

Figure 1 illustrates the basic exposure geometry, which represents an adaptation of the one photon proximity field nanopatterning (PnP)[13, 14] method. The figure also compares the optical response for the one and two photon cases as applied with a simple grating mask. The conformable phase masks are produced using the casting and curing procedures of soft lithography.[14] For the work presented here, these phase masks used ~5 mm thick composite elements of two types of the elastomer poly(dimethylsiloxane) (PDMS),[15] both of which are transparent for wavelengths between 300 nm and 1000 nm.[16] The relief structures on these masks consisted of posts with rounded square or circular cross sections, diagonal dimensions (d), heights (h) and center to center separations (p); mask 1: square array of circular posts (d=570 nm), h=510 nm, and p=710 nm, mask 2: square array of rounded square posts (d= 1000 nm), h= 510 nm, and p=1570 nm, mask 3: hexagonal array of circular posts (d= 1120 nm), h= 420 nm, and p=1500 nm. Due to their low moduli and surface energies, these elements can be brought into intimate, conformable contact with flat surfaces in a non-destructive, reversible manner.[17, 18] Contacting these elements with thin (~5-20 μm) solid layers of a commercially available epoxy photopolymer (SU8, Microchem Corp) on transparent glass substrates, and then shining light through the phase mask exposes the photopolymer to the well defined, 3D distributions in intensity created by passage of light through the mask. The SU8 can be crosslinked by exposure to ultraviolet light, through a one photon process,[19] or by exposure to high intensity near infrared light, through a two photon process.[20]

The collimated output (beam diameter ~600 μm) of a regeneratively amplified 1 kHz Ti:sapphire laser centered at 810 nm provided the high intensities needed for two photon patterning. At this spot size, pulse energies and durations of 250 μJ and 120 fs generate peak intensities of ~0.7 TW/cm2, which is in the range necessary to activate photocatalysts that induce crosslinking in the SU8. Exposure times between 120 to 240 seconds generated

sufficiently high concentrations of photocatalyst in the polymer at the locations of high intensity. Removing the phase mask, and then postbaking the SU8 (5 mins at 65C) crosslinked the exposed areas into an insoluble form; dissolving the unexposed areas away using a developer (SU-8 developer, Microchem Corp) and then supercritically drying the samples yielded free standing polymeric 3D structures. For comparison, we also generated, using similar steps, 3D structures using one photon effects with the 355 nm output of a tripled Nd:YAG laser.
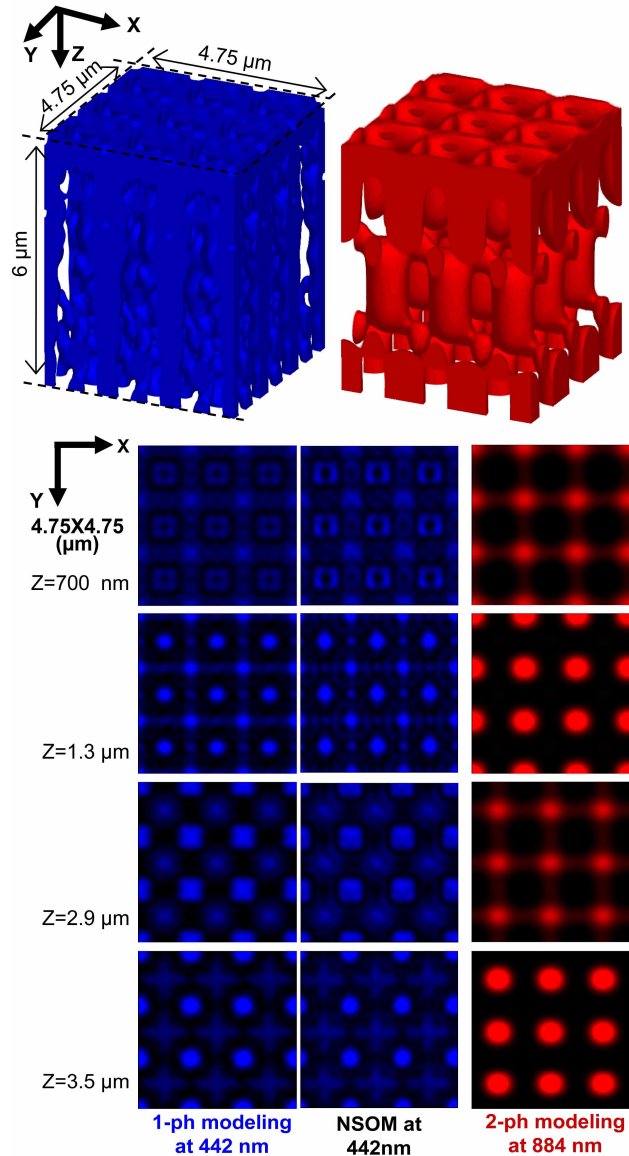
Fig. 2. Scanning optical measurements and modeling results of 3D distributions of intensity (left; wavelength of 442 nm) and the square of the intensity (right; wavelength of 884 nm) that result from passage of light through a 2D phase mask. The bottom frames show planar intensity distributions that correspond to the cases of calculated 1-photon (left; wavelength of 442 nm), measured 1-photon (middle; wavelength of 442 nm) and calculated 2-photon (right; wavelength of 884 nm). The mask, made of polyurethane (refractive index of 1.56), has a square array of rounded square holes (d= 1000 nm), h= 420 nm, and p=1570 nm.

Figure 1 schematically illustrates a simple experimental geometry to highlight differences between the one and two photon cases. The PDMS mask here (index of refraction = 1.4) consists of arrays of raised and recessed lines of relief with 1000 nm widths and relief depths of 510 nm. We assume, consistent with the experiments, that the substrate is transparent so that back reflections can be neglected. The figure shows results of simulations corresponding to 810 nm wavelengths (near infrared; NIR) in the one and two photon regimes and to 405 nm for the one photon case (deep blue). The calculations begin with full vector evaluation, using rigorous coupled wave analysis (RCWA)[21] of the phases. Consistent with Abbe theory of image formation,[22] the distribution of intensity near the surface of the mask (neglecting true near field effects) can be determined by evaluating the interference patterns formed by overlap of the far field diffracted beams. The results of such calculations show, as expected, striking differences between the one and two photon cases. These differences can be understood by considering that the diffraction angle, for a given mask, depends linearly on wavelength. Long wavelength light diffracts through larger angles and, therefore, produces fewer propagating diffracted beams than short wavelength light. For the case of Fig. 1, 810 nm light produces 3 diffracted orders (0th, +1st and -1st), while the 405 nm light produces 5 orders (0th, +1st, +2nd, -1st and -2nd). As a result, there are 3 and 5 spatial Fourier components in the 3D intensity distributions near the mask for 810 nm and 405 nm light, respectively. The lowest spatial frequencies in the cases (i.e. the frequency associated with interference of the 0th and 1st order beams) are, however, the same and are set by the geometry of the mask. Qualitatively, then, NIR light generates 3D distributions with less structure, but with the same dominant period (in plane), as deep blue light. The characteristic period of the 3D structures in the out of plane direction, known as the Talbot or self imaging distance, is given by $\lambda/[1-(1-\lambda^2/d^2)^{0.5}]$ (λ: wavelength, d: grating periodicity). This equation is an exact solution for $\lambda<d\leq2\lambda$, but is only approximate for $2\lambda<d$. This distance is, then, 4.73 μm and 1.96 μm for 405 nm and 810 nm light, respectively, for the mask considered here. Another important difference arises from the fact that the square of the intensity determines crosslinking in the two photon case whereas the intensity itself governs this process for a one photon interaction. The quadratic dependence improves the maximum optical contrast ratio (which, in turn, influences the ratio of the degree of crosslinking in the brightest to the darkest regions) and the ability to build 3D structures with open architectures. In fact, for the case of Fig. 1, the one photon contrast ratio for 810 nm light is $\sim6\times10^4$; the two photon contrast is $\sim3.5\times10^8$. The one photon contrast for 405 nm is $\sim1.5\times10^4$. The line cuts in the bottom frames of Fig. 1 illustrate this effect clearly. This quadratic intensity dependence also enables resolution that can exceed significantly the exposure wavelength, consistent with observations in conventional two photon patterning. The resulting resolution for 810 nm is, experimentally, only modestly less than for 405 nm.

Figure 2 shows similar simulations and scanning optical measurements (AlphaSNOM, WITec Instruments Corp.) of light passing through a mask with two dimensional arrays of relief features on its surfaces; the mask made of polyurethane (NOA 73, Norland Products) has square array of rounded square holes ((d= 1000 nm), h= 420 nm, and p= 1570 nm). Here, unlike in Fig. 1, the distributions of intensity have true 3D character, due to the 2D nature of the relief structures on the masks. The results, however, illustrate similar trends, qualitatively. The wavelength for the one photon case in Fig. 2 (experiments performed with the output of a continuous wave HeCd laser) was 442 nm. The two photon simulations were performed using a wavelength of 884 nm. The good agreement between the one photon measurements and simulations validates the calculation approach (for distances more than 100-200 nm from the surface of the mask). The top frames of this figure correspond to the solid form plots of intensity distributions after application of a binary cutoff filter that simulates, in a simple way, the crosslinking and developing process. The exposure dose and development time determine the appropriate position of this filter. This method for simulation ignores diffusion of developer and photocatalyst as well as many other details, but yields structure geometries that agree remarkably well with experiment, as described subsequently. The one and two photon

structures are the result of interference of 37 and 9 diffracted beams, respectively. The dominant in-plane periodicity is 710 nm for both cases, set by the geometry of the mask. The contrast ratio for the two photon 884 nm case ($\sim 1 \times 10^6$) is higher than that for the 442 nm case, in spite of the much lower diffraction efficiency of the mask for 884 nm than 442 nm light. The symmetry of the two photon 884 nm structure is body centered tetragonal with lattice parameters of a=1.57 μm and b=5.09 μm; smaller lattice parameters can be achieved easily by using masks with smaller features of relief as illustrated in the following.
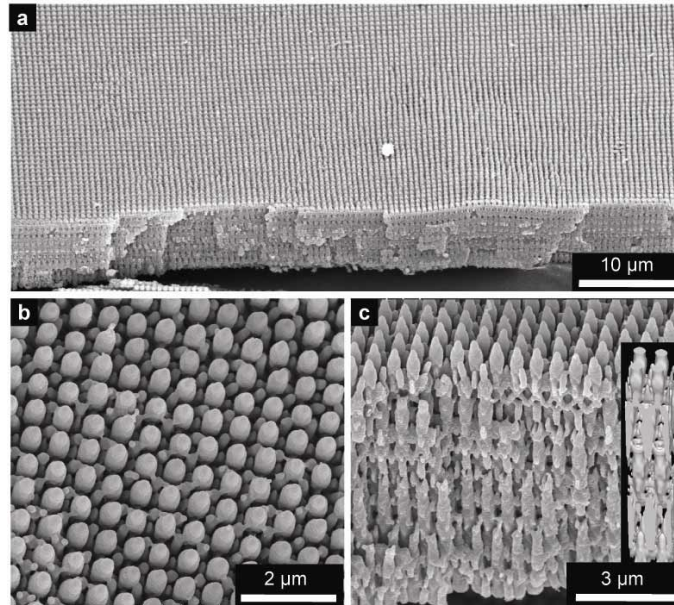
Fig. 3. SEM images and modeling of 3D structures made through a one photon process with mask 1 (d=570 nm, h=510 nm, p=710 nm, circular dot). (a) large area angled view, (b) top view, (c) cross sectional view and modeling (inset).

3. Experimental results and discussions

Figure 3 and 4 shows 3D structures of SU8 and calculations for the cases of one (355 nm) and two photon (810 nm) patterning with phase mask 1. Remarkably, although this mask (710 nm period) does not yield any diffracted beams when 810 nm light passes through it in open air, it generates well defined 3D structures in the SU8. Such patterning is possible because the index of the SU8 is large enough for diffracted beams to form in the SU8, where the 810 nm light has wavelength of 810/1.66 = 488 nm. Calculations indicate that 9 diffracted beams form in this case, compared to 37 for 355 nm light. The computed contrast ratio for the 810 nm light is ~30, corresponding to an effective contrast ratio of ~1000 for the two photon process. The contrast ratio at 355 nm is ~10000. As expected, the dominant in-plane periodicities of the one and two photon structures are similar, since they are set by the geometry of the phase mask. The depth variations of the geometries are, however, quite different, due to the different intensity distributions and interactions of the light with the polymer discussed previously. The two photon process in this case forms a simple body centered tetragonal (bct) structure, with geometries that are close to fcc; the lattice parameters are a=710 nm and b=1780 nm. The fill factor of these 3D structures can be adjusted by controlling the exposure and development times. In fact, for low exposure doses and/or long development times, it is possible to use the 810 nm two photon approach to produce large numbers of ellipsoidal particles of SU8. Figure 4(e) provides an image of such particles, and simulations generated with an appropriately defined cutoff filter.
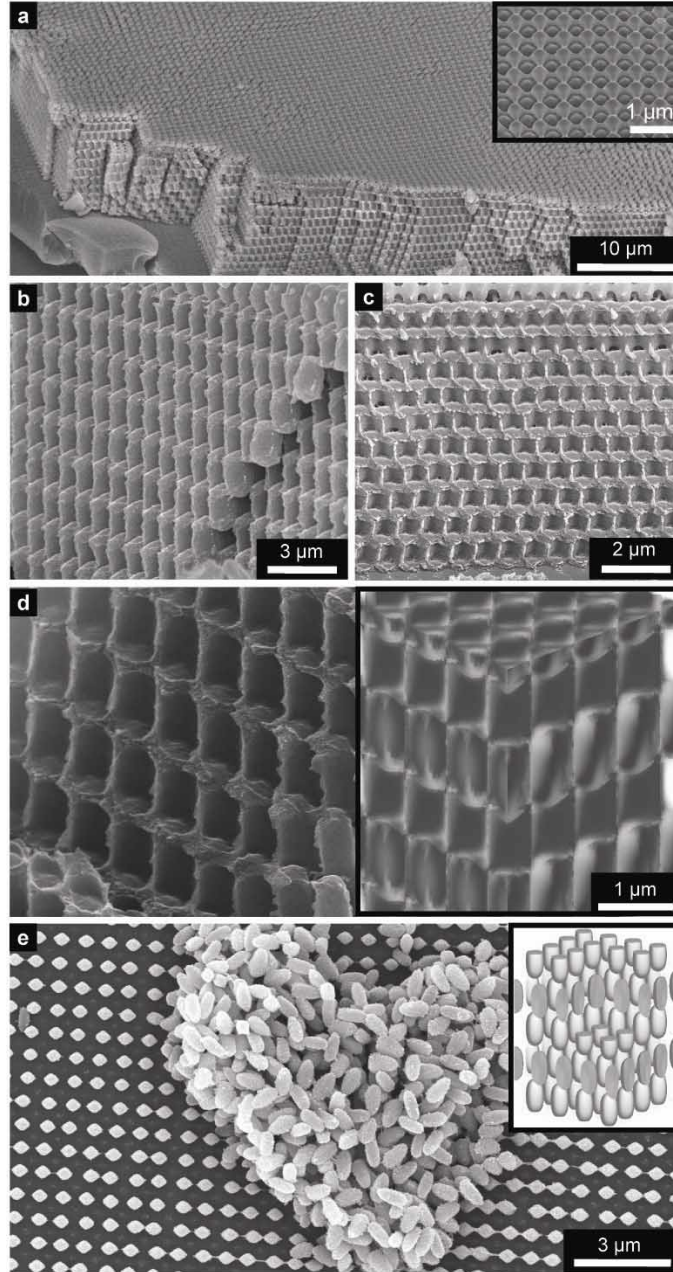
Fig. 4. SEM images and modeling of 3D structures made through a two photon process with mask 1 (a) large area angled view and top view (inset), (b) and (c) cross sectional views at different angles, (d) cross sectional view (left) and modeling (right), and (e) image of ellipsoidal particles and modeling (inset) made through a two photon process by use of a short exposure time (~60 sec). An appropriately defined cutoff filter, close to the experimental condition, is chosen for each modeling.

The sizes of the relief features on mask 1 used for the structures of Fig. 4 are much smaller than the wavelength of the 810 nm light. The mask itself, therefore, takes on optically anisotropic properties like a subwavelength optical element.[23] For the structures in Fig. 4, we used circularly polarized light to eliminate the effects of this anisotropy. By controlling

the state of polarization, it is possible to exploit the mask anisotropy to generate 3D structures with different geometries. Figure 5 presents images and corresponding simulations of the top surfaces of 3D structures made with the same mask, but using linearly polarized light with different orientations relative to the mask. These structures have distinct directionality along the polarization direction, which persists throughout their thicknesses and can be captured by the RCWA calculation approach. This level of polarization control over the geometries provides another fabrication design parameter.
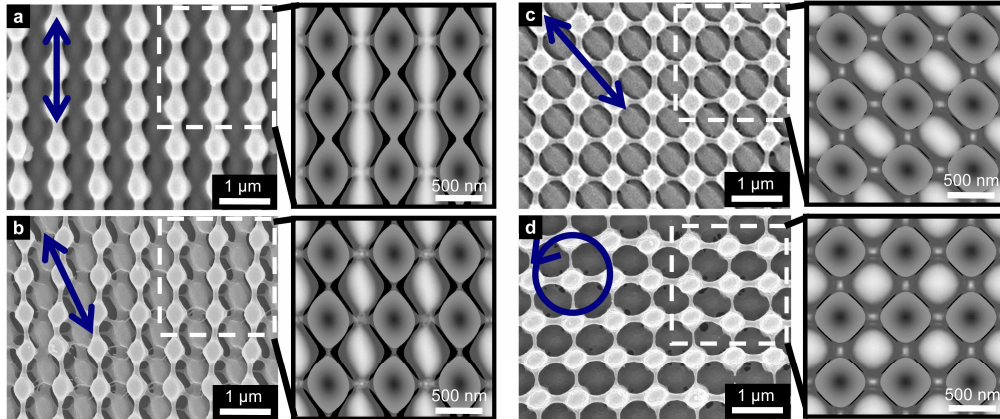
Fig. 5. SEM images of structures made through a two photon process with mask 1. Modeling results appear in the right column. The linear polarization of exposure light had angles of 0° (a), 22.5° (b), and 45° (c) relative to the [0, 1] direction of the mask. Frame (d) shows a corresponding structure formed with circularly polarized light.
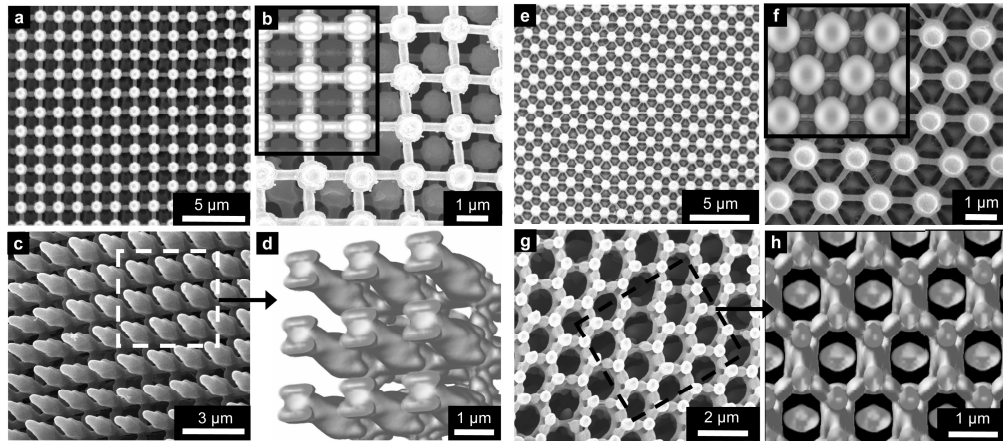
Fig. 6. (a-d) SEM images of structures made through a two photon process with mask 2 (square array of posts with, d= 1000 nm, h= 510 nm, p= 1570 nm, rounded square dot). (a) and (b) show images and modeling results (inset) of the surfaces. (c) and (d) show images and modeling, respectively, of an angled view of similar structures. (e-h) SEM images of structures made through a two photon process with mask 3 (triangular array of posts with, d= 1120 nm, h= 420 nm, p= 1500 nm, circular dot). Surface structure (e). Top surface comparison between modeling and sem (f), second layer (g) and corresponding 3D calculation (h).

The calculations quantitatively capture all of the observed behaviors illustrated in Figs. 3-5, but they do not include the effects of pulse duration and wavelength bandwidth. Spatial and temporal overlap of the fs pulses are guaranteed at the surface of the mask. The dispersion introduced by the grating and the differential pathlengths associated with wavelength dependent diffracted angles, however, create some broadening of the pulse and

other complications. For example, the 1st order diffracted beam for the case of Fig. 4 at the depth of z (μm) has a pathlength that is longer by ~0.37z than the 0th order. At a depth of 10 μm in photopolymer, there exists 3.7 μm of pathlength difference that is equivalent to ~12 fs of pulse duration, which decreases (but by a modest amount compared to the pulsewidth) the degree of overlap of the pulses. In addition, the pathlengths of the different wavelength components of pulses diffracted into a nonzero order are different; this effect temporally and spatially broadens the pulses. This broadening is, however, relatively small for distances of less than a few tens of microns from the surface of the mask. The situation is consistent with the good agreement between experiment and modeling; it is also intuitively reasonable when one considers that the spatial length of a 120 fs pulse is ~40 μm, which is considerably larger than the ~10 μm thick SU8 layers used here. Pulse broadening and imperfect overlap effects must be considered explicitly for thicknesses greater than ~40 μm.

In addition to the relatively simple 3D structures of Figs. 2, 4 and 5, the two photon process can generate complex 3D geometries. In particular, masks that have relief features with larger sizes lead to more structure in the intensity distributions, with high spatial frequencies and polarization independent behavior. Figure 6 presents 3D structures made using mask 2 (Fig. 6(a)-(d)) and mask 3 (Fig. 6(e)-(h)), both of which have periods (~1500 nm) large relative to 810 nm exposure wavelength. The highly open, 3D structures that result can be accurately modeled using the procedures described previously. In these systems, the minimum feature sizes are ~200 nm, which is more than four times smaller than the 810 nm exposure wavelength.

4. Conclusion

In summary, this paper presents a parallel, large area route to 3D nanostructures by two photon patterning in thick transparent photopolymers. Detailed modeling, using full vector calculations, quantitatively captures the key aspects of the method, and therefore represents a useful tool for designing phase masks for desired 3D structures. The geometries that can be achieved (some of which have the potential to be useful for applications in photonic bandgap materials, as well as various areas of microfluidics and drug release) and the simplicity of the method represent attractive features. The main disadvantage of the approach, compared to traditional two photon lithographic procedures, is its inability to produce structures with arbitrary geometries. The design of specialized (periodic or aperiodic) masks and/or multiple exposure steps to create an expanded range of 3D structures represents a topic of current work.

Acknowledgments